Bolton, M. D. & Powrie, W. (1988) *Géotechnique* **38**, No. 2, 167–189

Behaviour of diaphragm walls in clay prior to collapse

M. D. BOLTON* and W. POWRIE†

Centrifuge model tests have been used in an attempt to gain a coherent view of the soil–structure interaction behaviour following the excavation of soil in front of a pre-constructed wall. Excavation was simulated by the removal of a suitably heavy fluid from a preformed cavity. The broad replication of stress magnitudes and stress paths permitted the full representation of wall deformation, soil strain and swelling, completing a 50 year full-scale lifespan in under 24 hours of continuous centrifuging. Measurements were made of soil displacement vectors, pore water pressures, wall displacements and bending moments together with forces in props when they were present. These have made possible the validation of simplified 'geostructural mechanisms' which offer the same degree of advantage to the designer as does the idealization of beam behaviour encapsulated in engineer's beam theory. A serviceability criterion for soil or wall displacements can be entered into simplified admissible strain fields appropriate to the kinematic constraints so that the effective mobilized soil strain in the major zones of soil deformation can be deduced. This can lead, through triaxial or plane strain test data, to the selection of a mobilized soil strength and thence to an equilibrium analysis of the wall, from which unknowns such as the required wall penetration and bending strength and the required prop force can be determined. This approach leads to the evaluation of a design in terms of the chosen displacement criterion and avoids the question of defining or calculating a 'factor of safety'. Safety can be judged against separate collapse criteria, linked to the establishment of severe but realistic combinations of influences.

KEYWORDS: **diaphragm walls; deformation; centrifuge modelling; soil–structure interaction; design; time dependence.**

Des essais sur modèles en centrifugeuse furent employés pour une étude approfondie du comportement d'interaction sol/construction après l'excavation du sol devant un mur préconstruit. L'excavation fut simulée par l'enlèvement d'un fluide de pesanteur convenable à partir d'une cavité préformée. La reproduction essentielle des valeurs de contrainte et des chemins de contrainte permit en moins de 24 heures de centrifugeage continu la représentation complète de la déformation du mur et de la contrainte et du gonflement du sol qui auraient eu lieu en vraie grandeur pendant une période de 50 ans. Des mesures furent effectuées des vecteurs de déplacement du sol, des pressions de l'eau interstitielle, des déplacements du mur, des moments de flexion et des forces dans des supports éventuels. Des mécanismes géostructuraux furent ainsi validés qui offrent le même avantage aux constructeurs que l'idéalisation du comportement des poutres qui forme partie de la théorie des ingénieurs concernant les poutres. On peut introduire un critère d'application pour les déplacements du sol ou du mur dans des champs de contrainte admissibles simplifiés qui conviennent aux contraintes cinématiques de sorte quien puisse en déduire la contrainte effective du sol mobilisée dans les zones principales de la déformation du sol. Ceci peut conduire par moyen des données d'essais triaxiux ou de contrainte plane à une analyse d'équilibre du mur, à partir de laquelle des quantités inconnues peuvent se déterminer comme, par exemple, l'encastrement necessaire du mur, le moment de flexion et les efforts dans les buttons. Cette méthode conduit à l'évaluation d'un projet en fonction du critère de déplacement choisi et évite le problème de définir ou de calculer un facteur de sécurité. La sécurité peut s'évaluer en fonction des critères choisis d'effondrement combinés avec la définition de combinaisons strictes mais réalistes des influences.

Factors of safety may serve two purposes: to distance working states of a structure from conditions which would lead to collapse; and to ensure that working deflections are tolerable. In the design of rigid-plastic structures the former purpose would predominate, while the latter would be more important in the design of very flexible structures. As soil is particularly flexible and compressible in comparison with other construction materials, it may be that the avoidance of strain should supersede the avoidance of col-

Discussion on this Paper closes on 1 October 1988. For further details, see p. ii.

* University of Cambridge.
† King's College London.

lapse in geotechnical design evaluations and that 'factor of serviceability' should supplant 'factor of safety'.

It is recognised that the allowance of an undrained bearing pressure on clay of only $2c_u$, compared with an ultimate capacity of $5–6c_u$ arises mainly from the need to avoid significant plastic yielding in the soil under the edges of the footing, and settlements which would be very difficult to predict. Instead of referring to this problem as requiring a factor of safety of about 3, it would be more meaningful to speak of a serviceability factor of about 3 which is a prerequisite for simple elastic-type settlement calculations.

No such recognition exists in the design of retaining walls, which are conventionally designed using plastic analyses based on soil strength, without the benefit of any soil stiffness analysis. Serviceability is then guaranteed (hopefully) through the introduction of a factor of serviceability which is labelled as a factor of safety. It is sometimes applied in the form

$$F_s = \text{stabilizing forces/de-stabilizing forces} \quad (1)$$

This form is inherently unsatisfactory, because the stabilizing and de-stabilizing forces must always be exactly equal and opposite if the structure is to be in equilibrium. Furthermore, the frictional strength of soil increases if the applied load is increased, so it is unclear how one is to segregate the stabilizing and de-stabilizing effects.

Burland, Potts & Walsh (1981) discussed the problems of defining F_s for cantilever retaining walls and expressed the opinion that the most fundamental definition would be

$$F_s = \frac{\text{maximum soil strength}}{\text{mobilized soil strength}} \quad (2)$$

Considering that this would, in engineering practice, lead to unacceptable complications in design analysis, they created another definition using an analogy with bearing capacity calculations. This was held to be more acceptable than other formulations because it accorded most closely with the results from Eqn 2. However, the selection of a value for F_s in relation to the desired limitations on wall deformations is not obvious.

The objective of this Paper is to explore the potential of mobilized soil strength as the parameter for the control of deformations in cantilever retaining walls. The results of a number of centrifuge model tests on both propped and unpropped walls are introduced. Back analyses are made which take approximate account of each of the three components of a complete solution in solid mechanics—equilibrium, compatibility and a constitutive relationship. A method is then proposed by which a performance criterion in terms of wall or soil displacement can be converted into a soil strain limitation and thereby into a limitation on the soil strength which can be mobilized. Calculations identical in form to conventional collapse analyses can then be performed using only that mobilized soil strength which will not transgress the performance criterion for serviceability.

The tests were conducted on the Cambridge geotechnical centrifuge. Equivalent full-scale prototypes were stiff walls in overconsolidated kaolin, with a retained height of 10 m. The walls were either unpropped, or propped at the crest. Groundwater levels were initially at ground level and were generally kept high in the retained clay as the process of excavation was simulated. Displacements, pore water pressures, bending moments and prop forces were then monitored in the subsequent phase of softening following the relief of total stresses. Results are presented at prototype scale using a dimensionless time factor T_v to relate elapsed time to the timescale of pore water pressure equilibration. Values of T_v were calculated using the average length of the drainage path in the centrifuge model, and a coefficient of consolidation and swelling was deduced from measurements made during reconsolidation of the clay sample in the centrifuge.

A typical centrifuge model is illustrated in Fig. 1 and represents a section of a long retaining wall. The length of the model wall section was 150 mm, corresponding to 18·75 m of a prototype wall at a scale of 1:125. For ease of back-analysis, the deformation took place under conditions of plane strain. The plane vertical boundaries perpendicular to the face of the model wall should therefore have been rigid and frictionless. The centrifuge strong-box designed for the model tests had an aluminium alloy back-plate 16 mm thick with two horizontal stiffening beams, and a Perspex front window 80 mm thick. To reduce friction to a minimum, the inside of the backplate was well lubricated with silicone grease and the inside of the Perspex window was sprayed with a mould release agent so that the view of the model was not obscured. It was estimated that the total restraining force due to friction from all sources would be less than 10% of the typical fully active force (including porewater pressure) on the retained side of the model wall above excavation level (Powrie, 1986).

The clay used in the model tests was speswhite kaolin, chosen principally because of its relatively high permeability $k = 0{\cdot}8 \times 10^{-9}$ m/s (Al-Tabbaa, 1987). Kaolin powder was mixed with de-ionized water under a partial vacuum to a slurry with a moisture content of 120% (about twice the liquid limit). The slurry was then poured

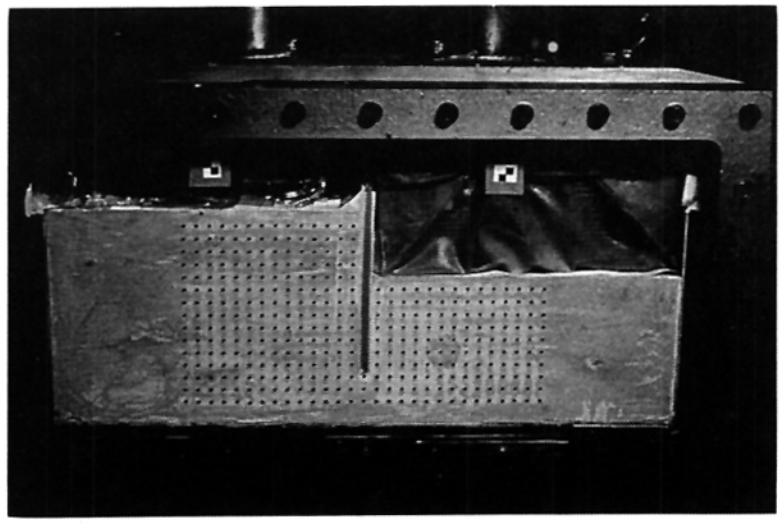

Fig. 1. Typical model (DWC 07) ready for testing in the centrifuge

into a consolidation press, where it was gradually compressed one-dimensionally to a vertical effective stress of 1250 kN/m^2 and then unloaded to a vertical effective stress of 80 kN/m^2.

At an average effective stress of just under 100 kN/m^2, the clay was removed from the consolidation press and cut to receive the model retaining wall. The excavation was also made at this stage. The clay removed was replaced by a rubber bag containing zinc chloride solution, mixed to the same unit weight as the clay and filled to the level of the retained ground. The model was then transferred to the centrifuge strong-box and instrumented. After an initial reconsolidation period, during which the clay sample came into equilibrium at 125 g under its enhanced self-weight, the zinc chloride solution was drained from the rubber bag in order to simulate the excavation of the soil in front of the wall.

The layout of the model and the instrumentation is shown in Fig. 2. In all tests, the retained

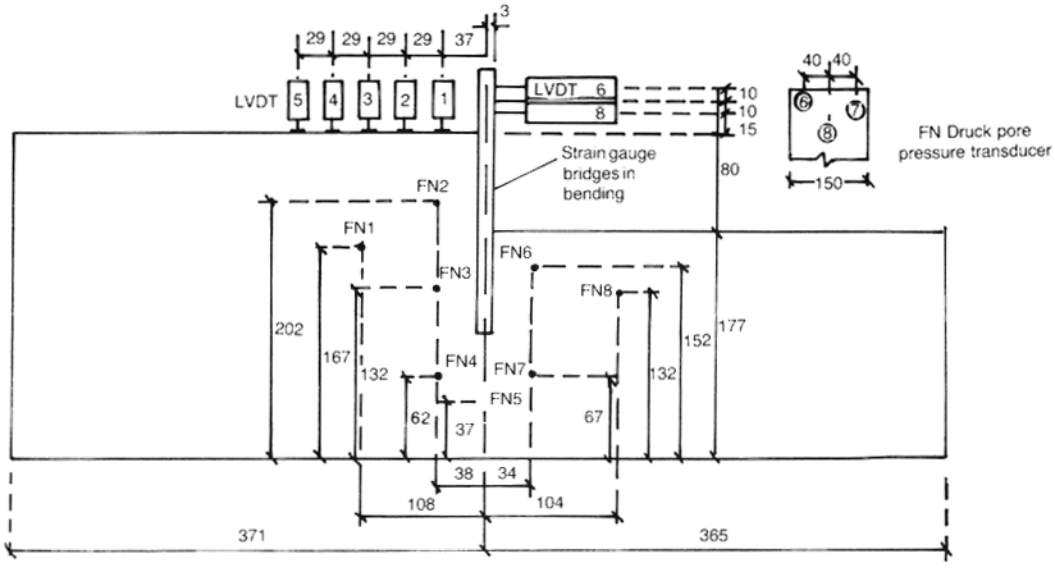

Fig. 2. Instrumentation of a typical model

height of 80 mm in the model represented 10 m at prototype scale. The model walls were intended to be impermeable to groundwater and effectively rigid in bending. They were made of either 9·5 mm or 4·7 mm aluminium alloy plate, giving equivalent bending stiffnesses EI at prototype scale of approximately 10^7 and $1{\cdot}2 \times 10^6$ kNm^2/m. The faces of the model walls were covered with a coating of resin 2 mm thick to protect the strain gauges and wires and to achieve a uniform and repeatable surface finish.

In most tests, a full height groundwater level on the retained side of the wall was modelled and special silicone rubber wiper seals were used to prevent water from leaking between the edges of the wall and the sides of the strong-box. Stand-pipes with overflow outlets at fixed elevations were supplied with water from hydraulic slip rings in order to create constant head devices. By adjusting the supply flow rate, the elevation of water above the stand-pipe outlet could be finely adjusted. During the initial reconsolidation, water was supplied at the elevation of the ground surface to the ground surface, a base drainage sheet, and the floor of the excavation. After excavation, solenoid valves were used to switch drainage lines so as to isolate the base drain and keep the water level in the excavation drawn down to the floor. It can be shown that the presence of the isolated drainage sheet at the base of the model caused the steady seepage solution to mimic that of a much deeper soil stratum. The general principles of centrifuge modelling are discussed in more detail by Schofield (1980), and the design of the model diaphragm wall tests is detailed in full by Powrie (1986). A companion paper (Bolton & Powrie, 1987) was concerned specifically with collapse limit states. Back-analyses were based on equilibrium stress fields which form the point of departure for the present study of deformations prior to collapse.

EQUILIBRIUM

Statically admissible stress fields are simplified stress distributions which are in equilibrium with gravity and any other applied loads, and which nowhere violate soil strength limitations usually embodied either by an effective angle of shearing resistance ϕ' or by an undrained strength c_u at a particular void ratio. Figure 3 shows one such stress field used (Bolton & Powrie, 1987) to back-analyse the collapse of unpropped cantilever walls. Frictionless surfaces are invoked on the wall surfaces and on the horizontal planes through the base of the wall and through an assumed pivot point about which active and passive soil zones were taken to switch over. Similar distributions were found to be reasonably

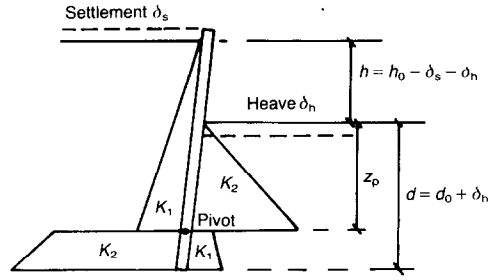

K_1 and K_2 are earth pressure coefficients
d_0 is the initial depth of embedment
$h_0 = 10$ m

Fig. 3. Admissible stress field for unpropped cantilever wall

accurate in back-analysis of cases of limiting stability.

Milligan & Bransby (1976) described the failure of sand retained by rigid model walls which were constrained to rotate about a point in their length. These authors investigated whether the stress discontinuity in the retained soil at the level of the pivot might be treated with a plastic fan zone, thereby enhancing the passive pressures by one or two orders of magnitude. They concluded that no theoretical stress distribution could convey the true situation, which depended on the mobilization of strain in the soil around and beneath the pivot. In their experiments, highly localized strains developed from the bottom edge of the wall, correlating with extremely strong passive stresses at the same point. The simpler stress field shown in Fig. 3 is preferred, as the required depth of wall below the pivot will be very small. It remains to be investigated whether this can lead to a useful estimate of mobilized strength and mobilized strain.

The focus of these approximate analyses is the equilibrium of the wall. Although points in the soil well away from the wall are taken to be in the same stress state as points on the same elevation near the wall, this is unrealistic. The plane dividing active and passive states would, if it were not frictionless, permit each zone to develop support from the other so that the state of stress in the soil would become safer further from the wall. This is ignored because it is not important for the stability of the wall; all that is desired from a limit-equilibrium standpoint is that a safe stress distribution be found.

It is assumed that stress distributions of the type shown in Fig. 3 are of relevance not only at collapse, but also in the phase of increasing strain prior to collapse. If a particular wall would be in limiting equilibrium with earth pressure coefficients corresponding to $\phi' = 20°$ in certain zones

it is assumed that the soil in these zones will uniformly mobilize 20° of its available angle of shearing even if that were to be somewhat larger, so that the wall was not on the point of failure. Such an assumption might seem unpromising. However, equilibrium is the essential condition leading to the selection of a value of mobilized strength. Only if the shape of the stress distribution prior to collapse were substantially different to that at failure would the assumption lead to significant error. This contingency can be investigated experimentally.

Non-linearity of the lateral stress distribution behind a wall propped near the crest was investigated by Rowe (1952, 1955). He defined an empirical soil stiffness constant m by the relation

$$\Delta\sigma = mz\,\Delta y/D \tag{3}$$

for the local increase in lateral stress due to a displacement Δy at depth z following the rotation or translation into the soil of a wall of embedment D. The bending stiffness of the wall was characterized by EI/H^4, or its inverse $\rho = H^4/EI$. Rowe's relative soil/structure stiffness was therefore

$$R = m\rho \tag{4}$$

It is not possible to relate the apparent soil stiffness m to any fundamental soil modulus. However, if in Eqn (3) $\Delta y/D$ can be treated as an approximate measure of local strain $\Delta\varepsilon$ it follows that

$$\Delta\sigma = mz\,\Delta\varepsilon \tag{5}$$

so that an equivalent Young's Modulus is

$$E = mz \tag{6}$$

To an order of magnitude therefore, m can be treated as the rate of increase of soil modulus with depth.

For the kaolin used in the models $m = 2000$ kN/m^3 at an axial strain of about 0·2% falling to about 1000 kN/m^3 at 0·5% strain. The more flexible retaining walls had a prototype bending stiffness of $1{\cdot}2 \times 10^6$ kNm^2/m and the stiffer walls, 10^7 kNm^2/m; this range brackets typical stiffnesses of existing walls. Prototype wall height (crest to foot) varied from 15 m to 30 m leading to a wall flexibility ρ between 0·7 and 0·005. The largest applicable soil/structure stiffness ratio would then be $R = 1350$ for the longest of the more flexibile walls generating small soil strains, but values a factor of ten or a hundred times smaller would be more typical of the tests as a whole. Rowe suggested that arching seriously affects the linearity of lateral stress diagrams only when $R \gg 1000$ in the case of such cantilever walls. Diaphragm walls propped near their crest may therefore be described as rigid rather than flexible, in relation to the clays which they support. However, relative soil/structure stiffness depends not only on the modulus of rigidity of the wall but also on its support conditions. Walls with extensible anchors, or multiple levels of anchors, or walls supported at the level of the excavation must each be considered separately.

A numerical analysis by Potts & Fourie (1984) based on elastic–frictional soil properties investigated the sensitivity of the pressure distribution behind a propped diaphragm wall to variations in the effective earth pressure coefficient K_0 prior to excavation. In particular, they showed that for a high initial K_0 of 2, the post-excavation earth pressures behind a typical diaphragm wall were far from linearly distributed. This was in strong contrast to their analysis for $K_0 = 0{\cdot}5$, which featured linear distributions of stress. However, the precise significance of this result is difficult to assess, as the analysis took no account of groundwater. An initial earth pressure coefficient of 2 corresponded to a rate of increase of effective lateral stress with depth of 40 kN/m^3. It has been argued (Powrie, 1985) that the process of construction of a diaphragm wall in clay would inevitably reduce K_0 towards unity prior to excavation. Furthermore, the presence of a high groundwater table would generally reduce the effective submerged unit weight of clay to less than 10 kN/m^3. A rate of increase of effective lateral stress of about 10 kN/m^3, corresponding to $K_0 = 0{\cdot}5$ in the Potts & Fourie analysis would appear to be more typical of real conditions. Their analysis therefore leaves open the question of whether stress distributions in practice might be approximated as linear for the purposes of design.

Equilibrium stress-field calculations based on linear stress distributions for walls propped rigidly at the crest are shown in Fig. 4. If the props do not fail, rotation of the wall must take place about the position of the props. The required depth of penetration follows from the condition of moment equilibrium about this axis, together with earth pressure coefficients based on the mobilized angle(s) of soil shearing.

The condition of moment equilibrium about the prop in Fig. 4 provides one equation in the two unknowns K_1, K_2 (see Appendix 1). One other equation is necessary to complete the solution. (The same applies to the unpropped wall in Fig. 3 which possesses both an extra unknown z_p locating the pivot point, and an extra equation of horizontal force equilibrium.) The missing relation could be provided using the assumption that

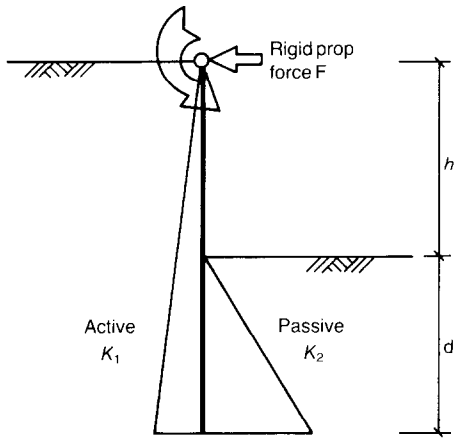

Fig. 4. Admissible stress field for wall propped at crest

mobilized angles of shearing in the two zones are equal

$$\phi'_{\text{mob 1}} = \phi'_{\text{mob 2}} \tag{7}$$

This might be justifiable for initial states $K_0 = 1$ if it was thought that equal strains would be induced in both regions, tending separately and symmetrically towards active and passive states. If the effects of wall friction were ignored, this elementary assumption would lead to the condition

$$K_1 = 1/K_2 \tag{8}$$

from which a solution to the mobilized earth pressures can be obtained by iteration.

Figure 5 shows the results of this elementary solution for ϕ'_{mob} in the case of a wall retaining 10 m of kaolin with full groundwater seepage. While, for example, an embedment of 20 m is vulnerable to drained failure with $\phi'_{\text{crit}} = 22°$, an embedment of 30 m reduces ϕ'_{mob} to 15°. This result is based on Eqn (8) which is as yet unsubstantiated. In order to substantiate statements about the degree of soil strength mobilized in various soil zones it is necessary to consider the mobilization of soil strain.

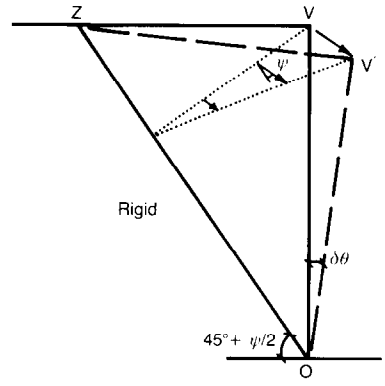

Fig. 6. Dilatant strain field, admissible for wall rotation about toe

COMPATIBILITY

Bransby & Milligan (1975) introduced a kinematically admissible soil strain field which was compatible with the outward rotation of a retaining wall. Figure 6 illustrates such a strain field in the simplest case of a soil shearing with a constant angle of dilatancy ψ behind a rigid wall pivoting at its base, O. A feature of these admissible strain fields is that the boundaries of the deforming regions are either zero-extension lines such as OZ in Fig. 6, or principal planes such as OV. As OV is the interface on the retaining wall, it is necessary to stipulate that the wall is frictionless. It was shown, however, that wall roughness had a negligible effect on the strain fields which emerged in model experiments. It was also shown that the increment in shear strain $\delta\gamma$ due to a wall rotation $\delta\theta$ is given by

$$\delta\gamma = 2 \sec \psi \delta\theta \tag{9}$$

This is insensitive to the dilatancy angle ψ; over the usual range, 0° for loose soil to 25° for dense soil, sec ψ varies only between 1·0 and 1·1.

Milligan & Bransby (1976) reported model tests in which a rigid wall retaining dense sand

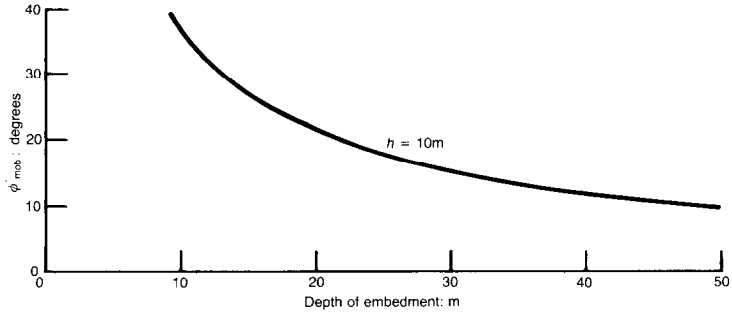

Fig. 5. Mobilized angle of shearing for frictionless walls, propped at crest, with full-height groundwater

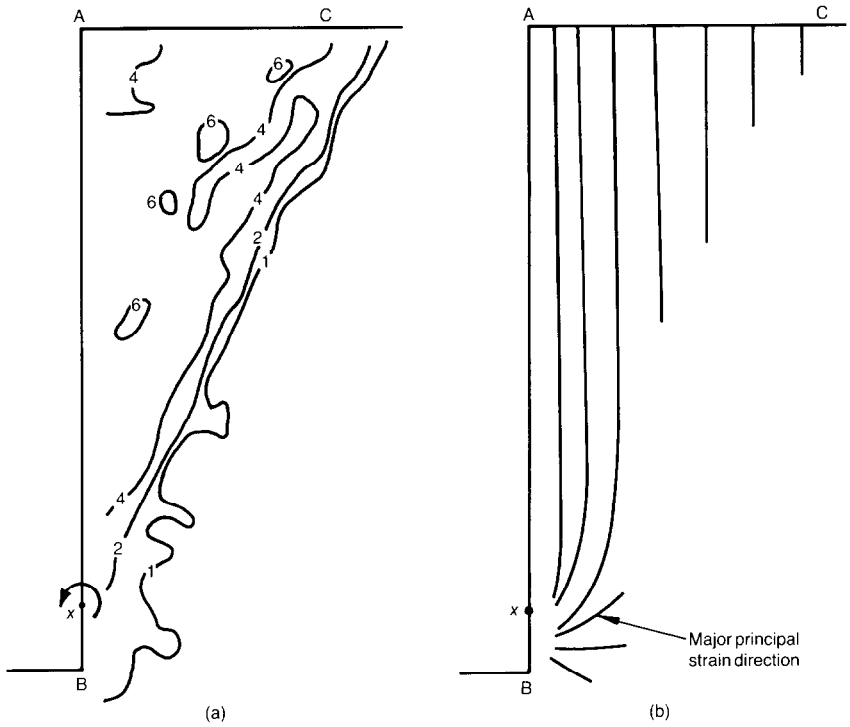

Fig. 7. After Milligan & Bransby (1976): (a) strain contours; (b) major principal strain directions in dense sand, following 1° wall rotation about x

was rotated about an axis contained within its own length. Figure 7(a) is their contour map of shear strain at a wall rotation $\theta = 1° = 1{\cdot}74\%$. Definition beneath the pivot was poor at small rotations, but the general shear strain of 4% in a triangular region above the pivot can be compared with Fig. 6 and the prediction $\delta\gamma = 3{\cdot}8\%$ (Eqn 9). In Fig. 7(b) the directions of principal compressive strain are seen to be vertical above the pivot and rotate towards the horizontal below the pivot, through a fan zone.

James, Smith & Bransby (1972) computed force/deformation solutions for the particular problem of the translation of a wall into soil, by stepping through consecutive plastic stress and strain field solutions portrayed using characteristics. This method could, in principle, be used to solve for any kinematic boundary conditions, but problems arise in computation where strong discontinuities or singularities have to be inserted into the net of characteristics.

The present objective is to enhance the stress fields shown in Figs 3 and 4 with equivalent admissible strain fields. A simpler approach is to subdivide the active and passive soil zones into triangles, the verticals and horizontals of which are frictionless displacement discontinuities while the hypotenuse of each is a zero extension line. It is necessary to select an angle of dilation for the clay. Zero dilation satisfies the undrained behaviour of clay. When permitted to drain, overconsolidated clay will initially shear quasi-elastically, but at higher stress ratios it will dilate until it ruptures. Shear softening will then occur until sufficient soil has reached a critical state. No further dilation will take place unless the change of geometry forces new rupture bands to develop. Since dilation is significant only in determining the size of the shear zone rather than the magnitude of strain within it, it was decided to impose the simplification $\psi = 0$ throughout.

Figure 8(a) depicts the simplified admissible strain field compatible with a frictionless rigid wall rotating outwards by a small angle $\delta\theta$ about its base. In the absence of dilation, zero-extension lines such as OA are at 45° to the principal directions, which must be vertical and horizontal. The uniform increment in horizontal strain $\delta\varepsilon_h$ inside triangle OVA can be calculated by the extension $h\delta\theta$ in AV

$$\delta\varepsilon_h = -h\delta\theta/h = -\delta\theta \qquad (10)$$

taking compression positive. The vertical strain increment $\delta\varepsilon_v$ can be calculated in this plane

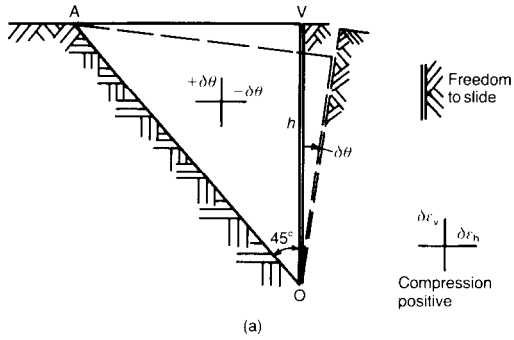

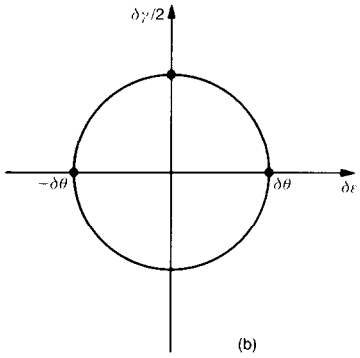

Fig. 8. Admissible strains for wall OV rotating about base: shear at constant volume

strain problem by invoking constancy of volume (zero rate of dilation) so that

$$\delta\varepsilon_v + \delta\varepsilon_h = 0 \tag{11}$$

$$\delta\varepsilon_v = +\delta\theta \tag{12}$$

Inward rotation would simply cause the signs of the vertical and horizontal strain increments to reverse. Figure 8(b) shows the corresponding Mohr diagram of strain increments. It will be seen that the increment of shear strain

$$\delta\gamma = 2\,\delta\theta \tag{13}$$

is in accordance with Eqn (9).

Figure 9 shows a similar strain field compatible with rotation of a wall about its crest V. The frictionless discontinuities have been moved to the opposite sides of an imaginary square ABOV drawn in the soil. Hypotenuse OA remains a zero extension line. That triangle AOV can remain rigid is demonstrable by considering the movement $(\delta u, \delta v)$ of a point P(x, y) on AO. Taking the strain increments in ABO from Eqns (10) and (12)

$$\delta u = +x\,\delta\theta$$

$$\delta v = -y\,\delta\theta$$

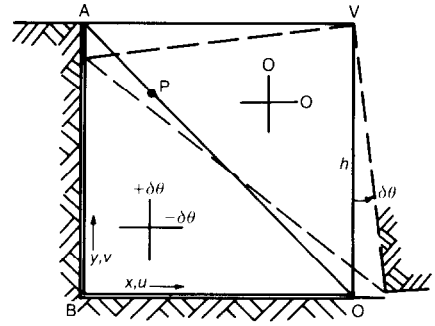

Fig. 9. Admissible strain field for wall rotating about crest

Substituting

$$y = h - x$$

it is found that

$$\frac{\delta u}{\delta v} = -\frac{x}{(h-x)} = -\frac{(h-y)}{(h-x)} \tag{14}$$

This is compatible with rigid body rotation of triangle AOV about V. The imposed rigidity of AOV and the artificial step created in the deformed soil surface at A, are compromises for the purpose of characterizing the actual mechanism. Once again, reversed passive rotation would simply lead to reversed strains.

Superposition of Figs 8 and 9 results in Fig. 10 for uniform strain within the square ABOV due to translation δu of the wall. Equal and opposite wall rotations $\delta\theta = \delta u/h$ about crest and base respectively give strain increments

$$\delta\varepsilon_h = -\delta u/h \tag{15}$$

$$\delta\varepsilon_v = +\delta u/h \tag{16}$$

and a shear strain increment

$$\delta\gamma = 2(\delta u/h) \tag{17}$$

everywhere within the square.

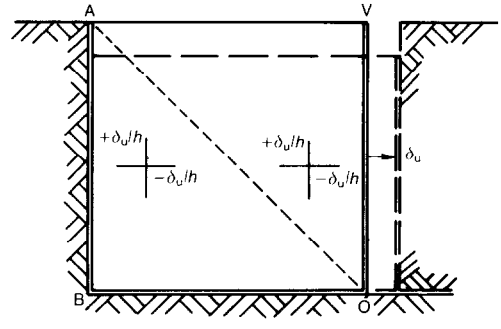

Fig. 10. Admissible strain field for wall in translation

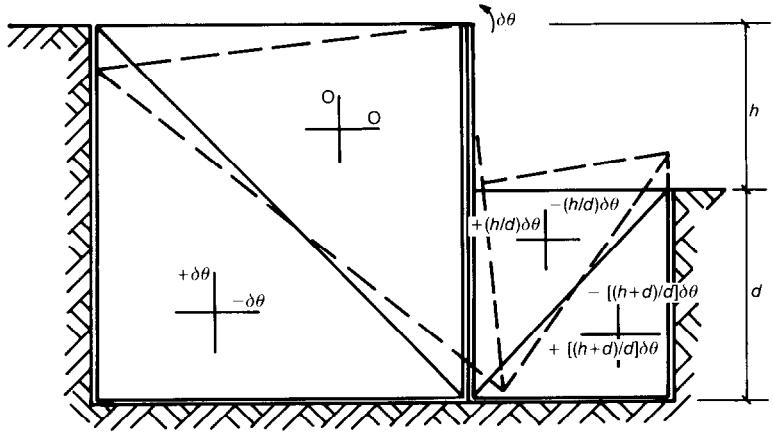

Fig. 11. Admissible strain field for embedded wall rotating about crest

The result of these admissible strain fields is that a wall rotation $\delta\theta$ can be seen to be consistent with an increment of soil shear strain $\delta\gamma = 2\delta\theta$ in a well defined zone of deformation irrespective of whether that rotation is inward or outward or whether it is about the crest or the base of the wall, and that translation of the wall can be synthesized by superposition.

Superposition of unequal components of Figs 8 & 9 results in a strain field compatible with a rotation about any desired point along the height of the wall. Although the two straining triangles do not conflict, the magnitudes of strain within them differ. However, if the objective is solely to extract a reasonable value for the ratio between mobilized shear strain and wall rotation, the larger of the two strains should suffice. This would be

$$\delta\gamma = 2\,\delta_{max}/h \tag{18}$$

where δ_{max} is the larger of the deflections of the wall at the top and bottom of the adjacent soil layer. For example, for the passive block in Fig. 11 restraining a rigid cantilever wall from rotation about its crest, Eqn (18) gives

$$\delta\gamma = 2(h + d/d)\delta\theta \tag{19}$$

With a typical ratio $d/h = 2$ this gives $\delta\gamma = 3\,\delta\theta$.

More complicated modes of wall deflexion can be derived either by the superposition of existing strain fields for the whole wall, or by the creation of a set of smaller compatible fields which suit a particular case and which can be assembled without violating the compatibility condition. For example, Fig. 12 shows an admissible strain field for an embedded cantilever wall VW of length L rotating by $\delta\theta$ about a point O, distance b from its base. Above O, an active triangle AOV and a passive triangle POQ are compatible with a frictionless wall element OV rotating about O. Below O, four triangles have been assembled which are compatible with a circulatory motion of the soil about the base W. For consistency, frictionless discontinuities have been inserted along both OS and RT to provide displacement discontinuities on these principal planes. The quadrants undergo a cyclic variation of state (passive–active–passive–active) from ORW anticlockwise to OTW. Again, the shear strain increment at any point is characterized as being either zero or 2 $\delta\theta$.

In comparing the strain increments in Fig. 12 with the stresses in Fig. 3, it can be seen that the imposed frictionless discontinuities coincide, and the directions of major principal stress and major principal strain increment also coincide for all zones of implied soil deformation in the vicinity of the wall. In all such zones a unique state of mobilized strength could be deduced from a given constitutive relation. In zones remote from the wall, where stresses were unrealistically 'unsafe', the soil is taken to be unrealistically rigid so as to compensate.

CONSTITUTIVE RELATIONSHIP

The strength and stiffness of a soil element is known to be a function of its effective stress history (particularly its maximum previous effective stress state), its present effective stress state, and its future state path (particularly in relation to any intended reversal or rotation of the principle strain direction). Soil is known to be anisotropic after one-dimensional consolidation during deposition and burial, and to be relatively stiff after each subsequent stress reversal. That this behaviour creates problems for the back analysis (or design) of soil constructions is clear (Ward,

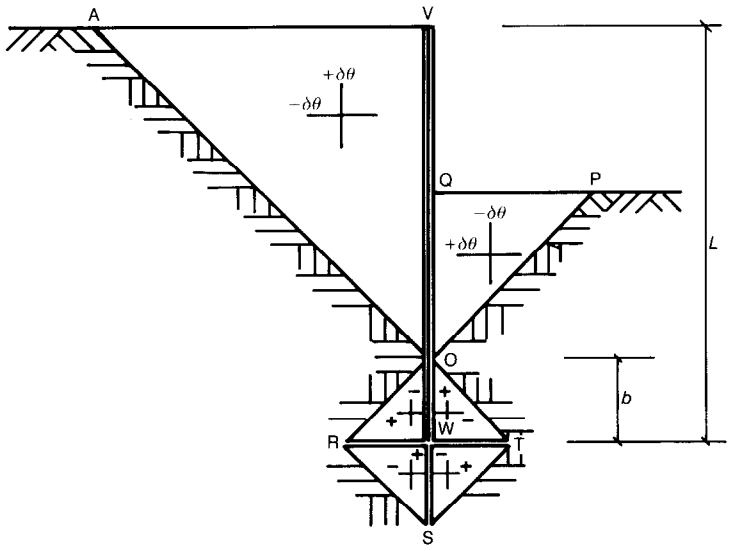

Fig. 12. Admissible strain field for unpropped wall

1961; Burland & Hancock, 1977; and Burland, Simpson & St John, 1979).

It could be considered that the typical ranges of stress around the walls in the present study correspond to 0–25 m of active soil and 0–15 m of passive soil. The range of minor effective stress would be 0–100 kN/m^2 on the active side and 0–120 kN/m^2 on the passive side, accounting approximately for pore pressures due to fully developed seepage around the wall. The range of effective cell pressure for testing should therefore have been of the order of 0–120 kN/m^2. At any particular stress level, two samples should have been tested in imitation of each of the active and passive strain regimes. Ideally, a variety of state paths would also have been employed, including undrained and drained tests and the increase and reduction of the mean effective stress as the deviatoric stress was increased in drained tests. All strain paths would approximate to plane strain. The principal advantage in the production of soil test data for the back analysis of laboratory models is that in every case the maximum effective vertical precompression of every soil element was known to be 1250 kN/m^2.

Conventional practice would demand only routine undrained triaxial compression tests with pore pressure measurement carried out on samples trimmed with vertical axes. It was decided to use this class of data and to enhance it with various exploratory tests (for example, at different OCR, or drained rather than undrained, or in plane strain rather than triaxial strain). Stress reversal was investigated only in terms of hysteresis loops derived from compression tests. The plane strain tests were carried out using a simple adapter fitted onto the base of a standard Wykeham Farrance triaxial test cell, as shown in Fig. 13.

A dimensionless constitutive relation would afford the best opportunity for generalization. Accordingly, a graph of secant mobilised ϕ' against shear strain γ (both defined in terms of a plane in the soil containing major and minor principal axes) was selected, so that

$$\phi' = \sin^{-1}[(\sigma_1' - \sigma_3')/(\sigma_1' + \sigma_3')] \quad (20)$$

$$\gamma = \varepsilon_1 - \varepsilon_3 \quad (21)$$

Figure 14(a) shows curves of ϕ'_{mob} against γ obtained from undrained triaxial tests on three samples, with initial overconsolidation ratios

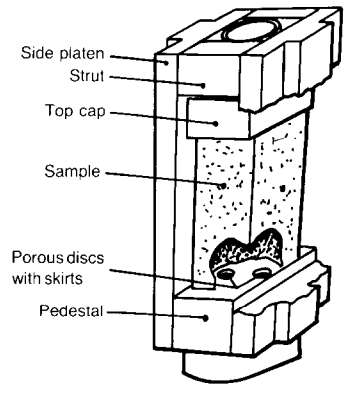

Fig. 13. Plane strain adaptation for triaxial cell

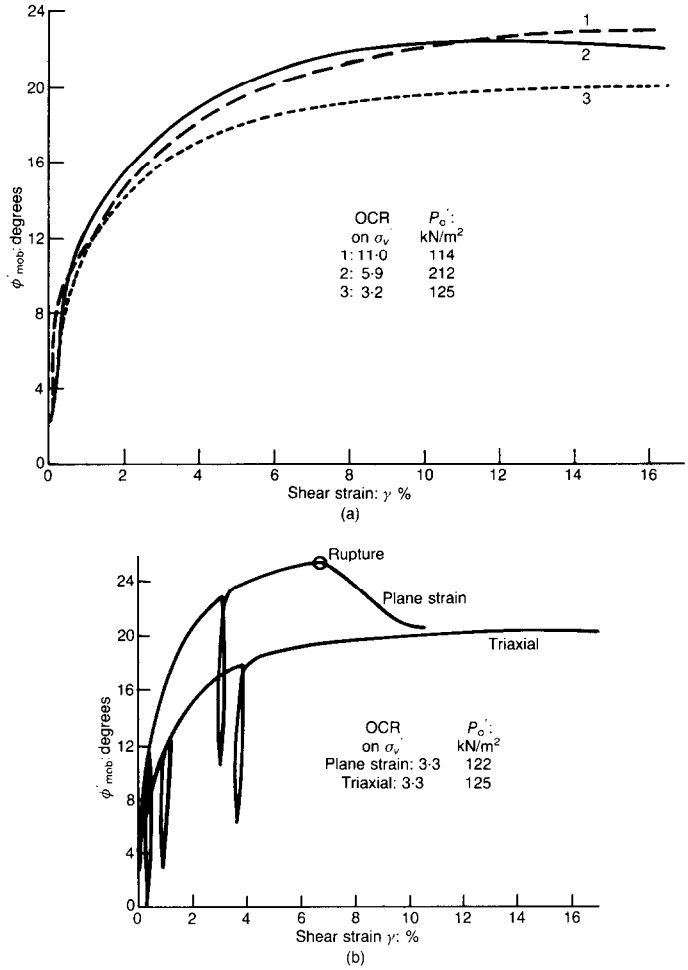

Fig. 14. Mobilized angle of shearing as a function of shear strain: (a) undrained triaxial compression tests from various OCR's; (b) undrained compression tests in plane and triaxial strain

(based on σ_v') of 11·0, 5·9 and 3·2. The secant stiffness ϕ'_{mob}/γ, at a mobilized angle of shearing of 18° varied by less than 30%. In contrast, Fig. 14(b) indicates that at $\phi'_{mob} = 18°$, the secant stiffness of similar samples tested in plane strain and under triaxial conditions differed by a factor of three. Apparently, triaxial data errs on the safe side rather more than should be tolerated.

Figure 15(a) shows the effective stress paths in q–p' space followed in drained and undrained triaxial tests on two samples with initially similar stress histories. The relationship between the corresponding ϕ'_{mob}–γ curves shown in Fig. 15(b) is as expected, the undrained path leading to somewhat larger strains as it traverses through states of high stress ratio at a reduced mean effective stress. Soil elements, in either the model or the field, initially suffer undrained shear strains on excavation, followed by the drained phase of pore pressure equilibration which can lead to additional shear strains. The lowest credible stiffness should be used in design. It was therefore considered appropriate to use the ϕ'_{mob}–γ curve obtained from the undrained plane strain test (Fig. 14(b)) with a relatively low initial OCR of 3·3, to calculate the soil displacements projected by the proposed design methodology.

UNPROPPED WALLS

It is possible for a wall which is initially stable to collapse gradually as the excess pore water suctions induced on excavation dissipate and

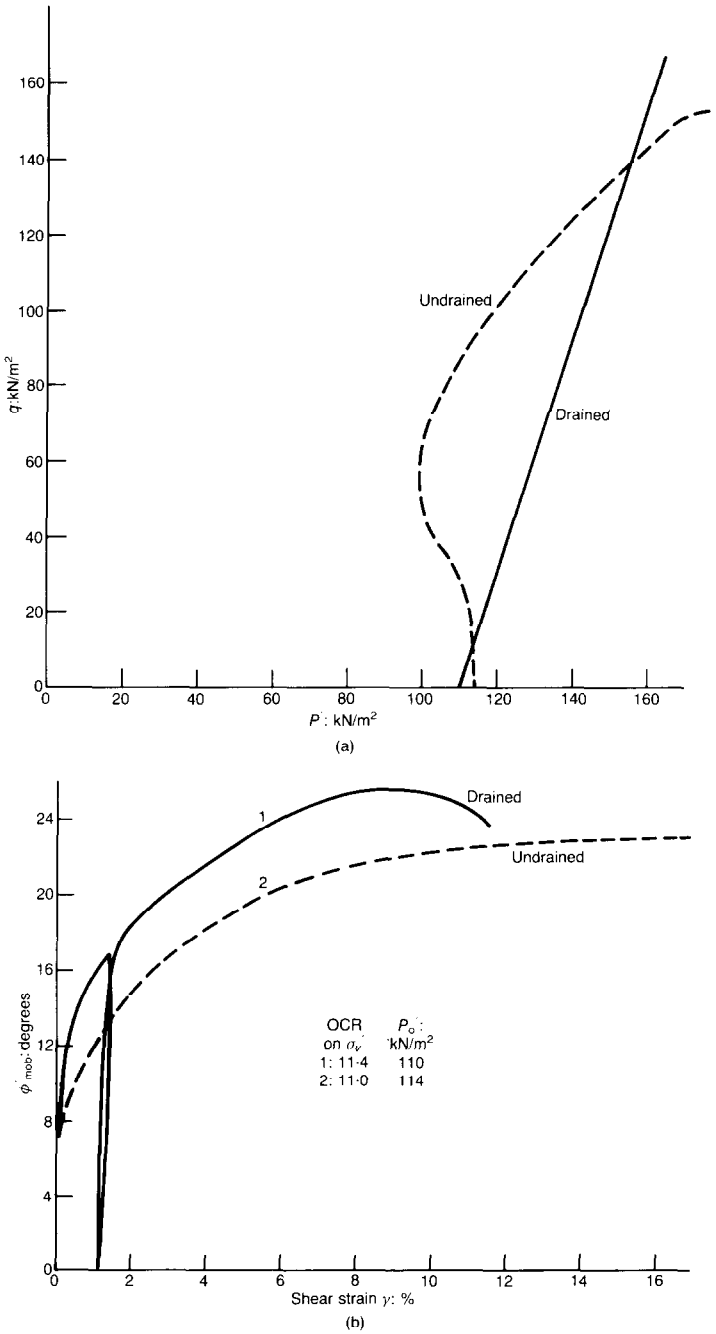

Fig. 15. Comparison between drained and undrained triaxial tests: (a) stress paths; (b) mobilized angle of shearing as a function of shear strain

steady-state seepage is approached. This class of behaviour was observed in two of the tests on unpropped model walls reported by Bolton & Powrie (1987): test DWC07 (10 m retained height, 15 m penetration) and test DWC08 (10 m retained height, 20 m penetration). In the case of the centrifuge model test, the pore water pressures were measured and the effective stress equilibrium analysis shown in Fig. 3 can be applied at any stage to calculate the mobilized angle of soil fric-

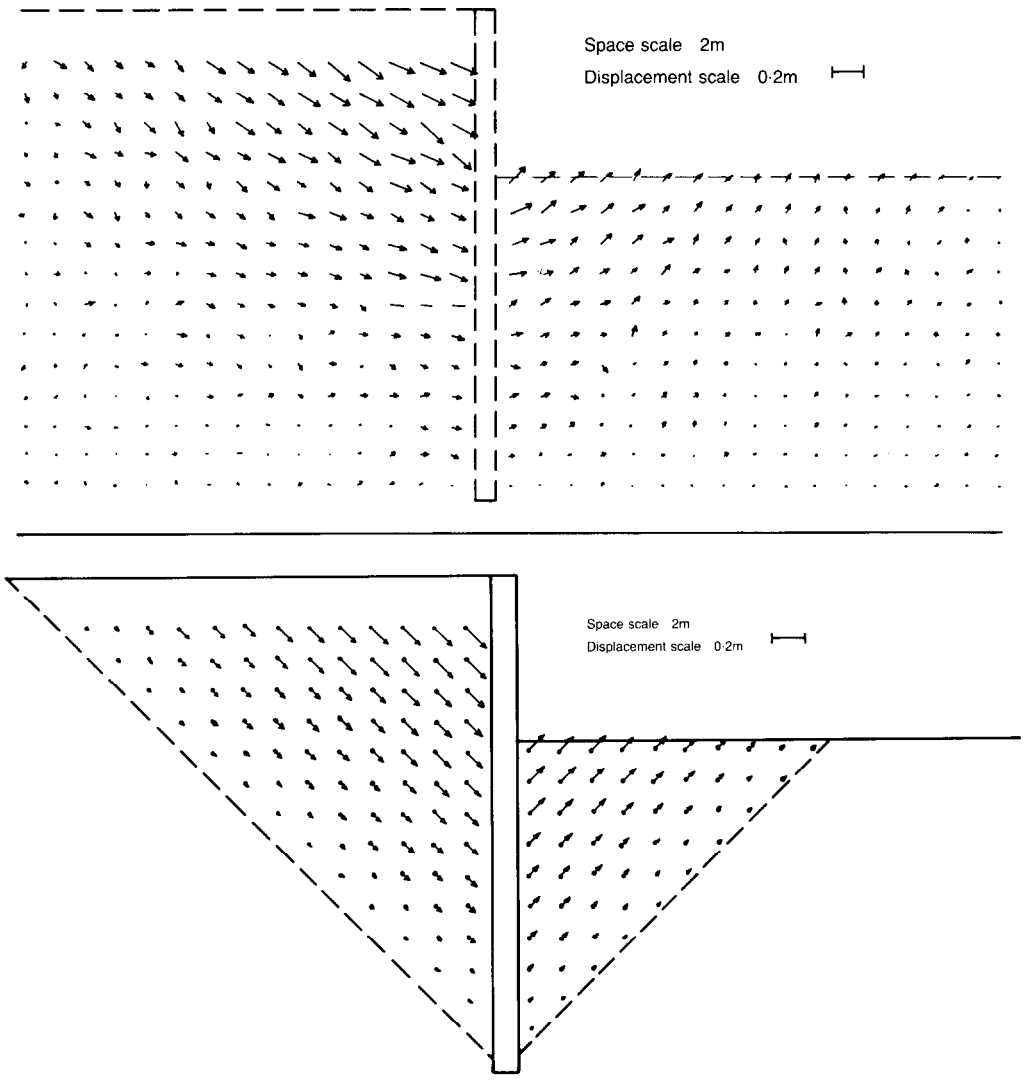

Fig. 16. (a) Soil movements during excavation, test DWC08; (b) calculated displacements during excavation, test DWC08

tion. A corresponding shear strain can then be deduced and displacements would follow from the shear strain mechanism shown in Fig. 12.

These stress and strain fields are applicable only to a smooth wall, and may overpredict the displacements of a rough wall. In this case an entirely empirical adjustment can be made, using the modified earth pressure coefficients given by Caquot & Kerisel (1948) to derive ϕ'_{mob}, but taking the relationship between wall rotation $\delta\theta$ and characteristic shear strain $\delta\gamma$ to remain unaffected, i.e. $\delta\gamma = 2\ \delta\theta$.

In the strain field shown in Fig. 12, deformation is supposed to take place at constant volume. A first order correction for volumetric strains would be to superimpose one-dimensional consolidation or swelling effects due to the changes in pore water pressure. A more thorough treatment would involve the careful segregation of elastic and plastic strain increments, and the use of a dilatancy relationship between plastic components of volumetric and shear strains. The admissible strain fields would then have to be modified to take dilation into account. This more rigorous approach was considered not to be justified unless the model test data indicated that the simpler analysis was in gross error.

An equilibrium calculation following Fig. 3

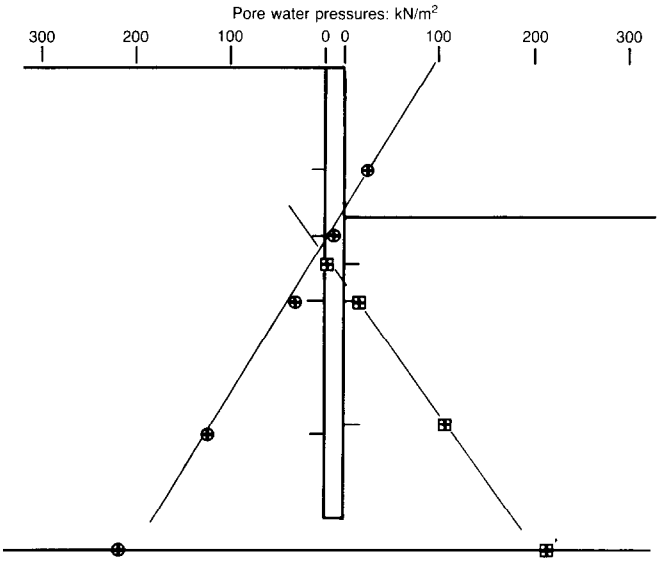

Fig. 17. Pore water pressures around the wall, 12·3 years after excavation, test DWC22

based on the undeformed wall geometry and the pore water pressures measured at the end of excavation in test DWC 08, indicates that a mobilized angle of shearing of approximately 17·5° is required with $\delta = \phi'_{mob}$, or a mobilized angle of shearing of just over 23° if the effect of wall friction is neglected ($\delta = 0$). The corresponding shear strains from Fig. 14(b) are 1·1% and 3·5% respectively, and the depth to the pivot z_p is approximately 18·8 m in both cases, leading to crest deflexions of 158 mm and 504 mm. Figure 16 shows that the displacements measured from photographs of the markers visible in Fig. 1 are similar to those calculated using the strain field shown in Fig. 12 with a characteristic shear strain of 1·1%. Displacements calculated using a characteristic shear strain of 3·5% would be much larger than those measured, which implies that in this case there was sufficient movement to mobilize full friction $\delta = \phi'_{mob}$ at the soil–wall interface.

The long-term deformations which occurred during centrifuge test DWC08 would probably be unacceptable in a prototype structure. The behaviour of an unpropped wall of the same geometry (10 m retained height, 20 m depth of embedment) but with a lower groundwater level, was investigated in test DWC22. The pore water pressures measured 12·3 years after excavation at prototype scale ($T_v = 1·3$) are shown in Fig. 17. Under these groundwater conditions, the equilibrium calculation shown in Fig. 3 indicates a mobilized angle of shearing of 13·5° ($\delta = \phi'_{mob}$) or 17·8° ($\delta = 0$). The depth to the pivot z_p is approximately 19 m in both cases and the corresponding shear strains of 0·6% ($\delta = \phi'_{mob}$) and 1·2% ($\delta = 0$) yield calculated tip deflexions of 86 mm and 172 mm respectively. The observed deflexion was 126 mm at prototype scale, which lies within the calculated range. These calculations are summarized in Table 1.

Table 1. Summary of equilibrium calculations for unpropped walls of 20 m embedment

Time factor: T_v	Input parameters		Calculated parameters		Crest deflexion: mm	
	Pore water pressures	δ/ϕ'	ϕ'_{mob}	γ	Predicted	Measured
0	Measured, DWC08	0 1	23·0° 17·5°	3·5% 1·1%	504 158	170
1·3	Measured, DWC22 (Fig. 17)	0 1	17·8° 13·5°	1·2% 0·6%	172 86	126

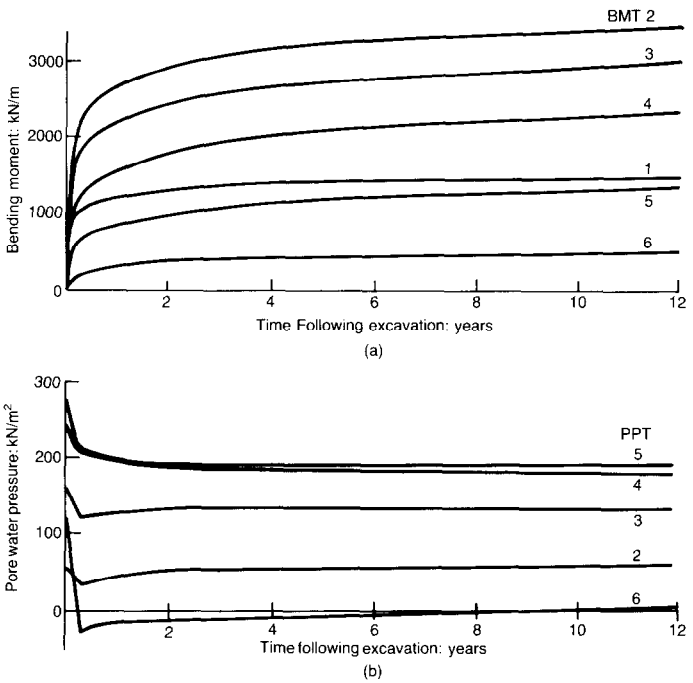

Fig. 18. Transient response (scaled-up), test DWC16

WALLS PROPPED AT THE CREST

The model wall used in test DWC16 was propped at the crest, and represented a retained height of 10 m, a depth of embedment of 15 m and a bending stiffness EI of $1{\cdot}2 \times 10^6$ kNm^2/m at prototype scale. Under the prevailing groundwater conditions measured at the end of the test, the mobilized angle of shearing for a smooth wall ($\delta = 0$) according to the calculation in Fig. 4 is 21·3°. If the wall is rough ($\delta = \phi'$), the mobilized angle of shearing can be estimated from the earth pressure coefficients given by Caquot & Kerisel (1948) and reduced to 15·8°. Thus the wall would certainly not be expected to have collapsed outright.

The bending moments measured during test DWC16 are shown as functions of time in Fig. 18(a). The gradual increase in the bending moments (and prop forces) is directly attributable to the readjustment of the pore water pressures to their long-term equilibrium values, and in particular to the dissipation of the excess pore water suctions induced in the soil on excavation (Fig. 18(b)).

The pore water pressures measured near the model wall at two separate instants during the test are recorded in Fig. 19(a). The first instant was shortly after excavation, and the second was near the end of the test after 12·3 years would have elapsed at prototype scale ($T_v = 1{\cdot}3$) and steady seepage established. The idealized linear pore water pressure distributions shown in Fig. 19(a) were used in the back analysis of the model test. In Fig. 19(b), the pore water pressures measured after 12·3 years at prototype scale are compared with the values obtained from the idealized steady-state flow-net for seepage from a full height groundwater level behind the wall to a wetted surface within the excavation. It may be noted that the idealized groundwater conditions were not replicated exactly in the model test, but were closer to those which might be expected in practice with a reduced groundwater level on the excavated side of the wall.

The bending moments measured in the model wall at these two instants are shown (at prototype scale) in Fig. 20, together with the corresponding prop forces. Computed bending moment diagrams are also shown. These were calculated on the assumption that the effective lateral earth pressure is proportional to the depth below the soil surface, and that the wall is perfectly rough, i.e. $\delta = \phi'_{\text{mob}}$. For a wall propped at the crest, the admissible strain field (Fig. 11) indicates that for a given wall rotation θ, the maximum shear strain on the retained side is 2θ, and that on the excavated side is $2\theta\ (1 + h/d)$. In this case, $h = 10$ m and $d = 15$ m and the maximum shear strain on the excavated side is 5/3 greater than that on the retained side. Accordingly, the moment equi-

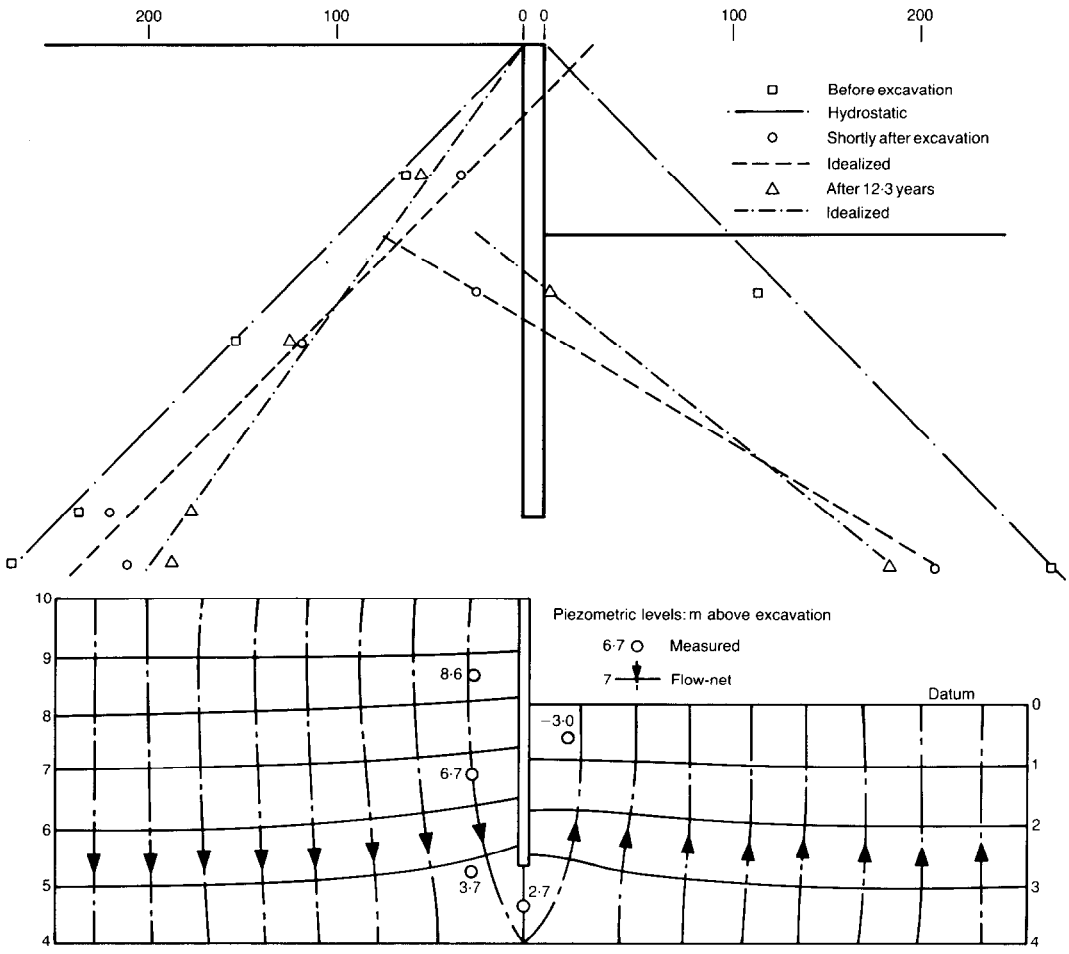

Fig. 19. (a) Pore water pressures measured around wall, test DWC16; (b) piezometric levels, test DWC16, after 12·3 years

librium calculation for the earth pressure coefficients K_1 (on the retained side) and K_2 (on the excavated side) was repeated until a pair of values was found corresponding to mobilized angles of shearing on each side of the wall which would be consistent (Fig. 14(b)) with this difference in characteristic shear strain. The measured pore water pressures were introduced into the calculation by means of the linear idealizations shown in Fig. 19(a). The prop load was then obtained from the condition of horizontal equilibrium, and the bending moments were calculated from the loads on the wall in the normal way.

Figure 20 shows that the bending moments measured just after excavation in test DWC16 are close to those calculated using this method with $K_1 = 0{\cdot}57$ and $K_2 = 2{\cdot}22$, which correspond to $\delta = \phi' = 12{\cdot}5°$ and $\gamma = 0{\cdot}5\%$ on the retained side, and $\delta = \phi' = 15{\cdot}9°$ and $\gamma = 0{\cdot}8\%$ on the excavated side of the wall. After 12·3 years at prototype scale ($T_v = 1{\cdot}3$) the measured bending moments are close to those calculated using $K_1 = 0{\cdot}55$ ($\delta = \phi' = 13{\cdot}5°$, $\gamma = 0{\cdot}55\%$) and $K_2 = 2{\cdot}35$ ($\delta = \phi' = 16{\cdot}8°$, $\gamma = 0{\cdot}95\%$). The measured and computed prop loads are also in agreement. These calculations are summarized in Table 2.

If the analysis had been simplified by making the assumption $K_1 = 1/K_2$, the calculated bending moments would not have differed by more than 4%. In some cases, this assumption could usefully be made without introducing any significant error.

Figure 21 shows the soil displacements (measured from photographs) which occurred during excavation. The horizontal movement of the retained soil near the top of the wall was larger than would be expected for a wall propped rigidly at its crest. This was due to a lack of contact between the wall and the props at the start of the excavation process. While every care

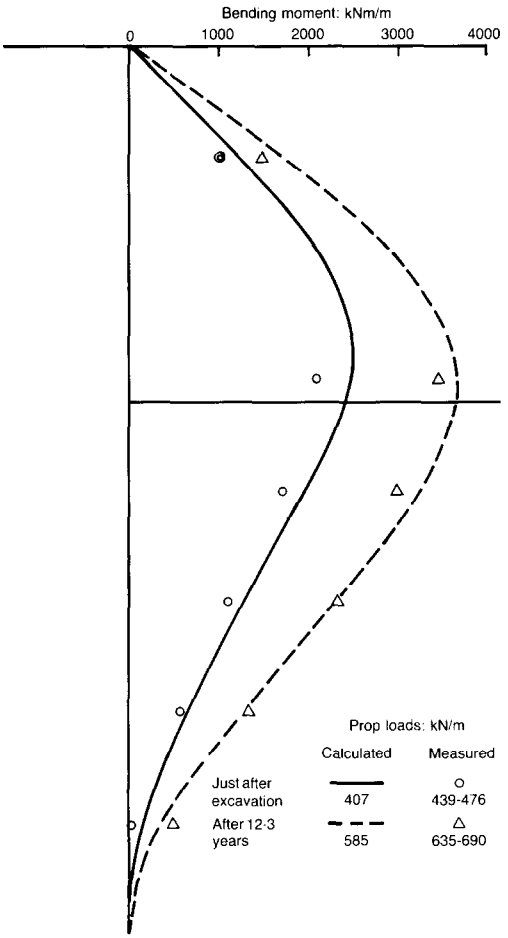

Fig. 20. Bending moments and prop forces, test DWC16, at 12·3 years prototype scale

was taken to ensure that the props were correctly placed, no control could be exercised over relative movements between the wall and the props during reconsolidation in the centrifuge. During excavation, the top of the wall moved forwards by just under 0·6 mm, which corresponds to about 70 mm at prototype scale. The effect of this lack of fit is not taken into account by the admissible strain field shown in Fig. 11. Therefore, the displacements measured in centrifuge test DWC14, on a wall of similar geometry but with a bending stiffness at prototype scale of 10^7 kNm^2/m which was rigidly propped at the crest, will be compared with those calculated using the equilibrium calculation and admissible strain field already described.

According to the stress field analysis shown in Fig. 4, the wall of test DWC14 would be in equilibrium with the pore water pressures measured immediately after excavation and soil stresses given by earth pressure coefficients $K_1 = 0{\cdot}47$ and $K_2 = 2{\cdot}85$. These coefficients correspond to $\delta = \phi' = 17{\cdot}25°$ and $\gamma = 1{\cdot}05\%$ on the retained side, and $\delta = \phi' = 20{\cdot}1°$ and $\gamma = 1{\cdot}72\%$ on the excavated side of the wall. If the effects of wall friction are neglected, the equilibrium earth pressure coefficients become $K_1 = 0{\cdot}44$ ($\phi' = 23°$, $\gamma = 3{\cdot}1\%$) and $K_2 = 2{\cdot}46$ ($\phi' = 25°$, $\gamma = 5\%$).

The measured and calculated soil settlements are compared in Fig. 22. As with the unpropped wall used in test DWC08, the actual settlements are closer to those calculated using the smaller characteristic shear strains, on the assumption $\delta = \phi'_{mob}$. It is unlikely that long-term displacements of the magnitude observed in the centrifuge tests would be acceptable in a prototype structure, which would probably be designed to a lower mobilized soil strength.

The methods used for the back-analysis of events which have already occurred can be

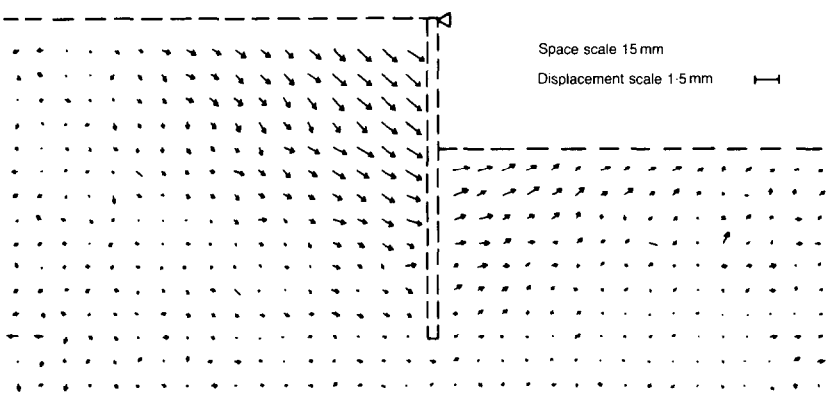

Fig. 21. Soil movements during excavation, test DWC16

Table 2. Summary of equilibrium calculations for test DWC16 (15 m embedment propped at the crest)

Time factor	Input parameters			Calculated parameters				Prop force: kN/m		Maximum bending moment: kNm/m	
				Retained side		Excavated side					
T_v	Pore water pressures	δ/ϕ'	Other	ϕ'_{mob}	γ_r	ϕ'_{mob}	γ_e	Predicted	Measured	Predicted	Measured
0	Test DWC16 (Fig. 18)	1	$\gamma_e = 5\gamma_r/3$	12·5°	0·5%	15·9°	0·8%	407	439–476	2468	2104
			$K_1 = 1/K_2$	16·1°	0·86%	14·4°	0·69%	374		2430	
1·3	Test DWC16 (Fig. 18)	1	$\gamma_e = 5\gamma_r/3$	13·5°	0·55%	16·8°	0·95%	585	635–690	3588	3503
			$K_1 = 1/K_2$	17·1°	1·03%	15·2°	0·77%	555		3550	

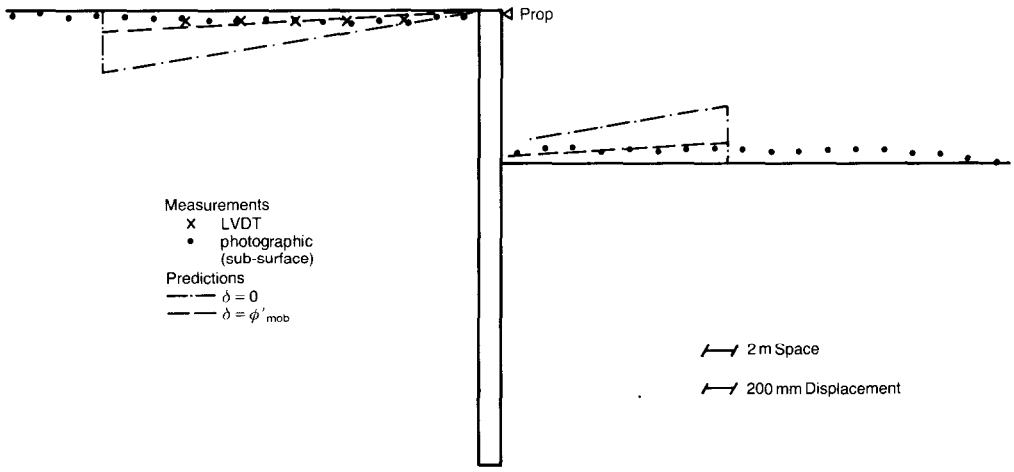

Fig. 22. Measured and calculated settlements, DWC14

applied to design, but the approach would differ slightly in two respects. First, depending on the pre-excavation soil stresses and the proposed method of construction, it may be appropriate to invoke a different relationship between the angles of soil friction on each side of the wall. This would be based on in situ test data for K_0 and laboratory test data for ϕ' as a function of shear strain.

Second, the pore water pressures must be predicted, perhaps using the methods suggested previously and in Appendix 2. Alternatively, a short-term analysis might proceed in terms of a mobilized shear strength c_{mob} as described by Bolton *et al.* (1987). The transient pore water suctions induced on excavation are a function of the structural stiffness. If the soil is assumed to be isotropic and reversibly elastic, the transient pore water pressures can be estimated from the condition that $p' =$ constant. The long-term pore water pressures are dominated by seepage, and are therefore a function of geometry and not of structural stiffness; they can be estimated easily enough from a flow-net.

The side walls of the M25 motorway tunnel at Bell Common, south of Epping, were constructed in situ using the secant pile technique, and act as embedded cantilevers, propped near the crest by the roof slab. The performance of one side wall is currently monitored by the Transport and Road Research Laboratory (TRRL) and the Building Research Establishment (BRE).

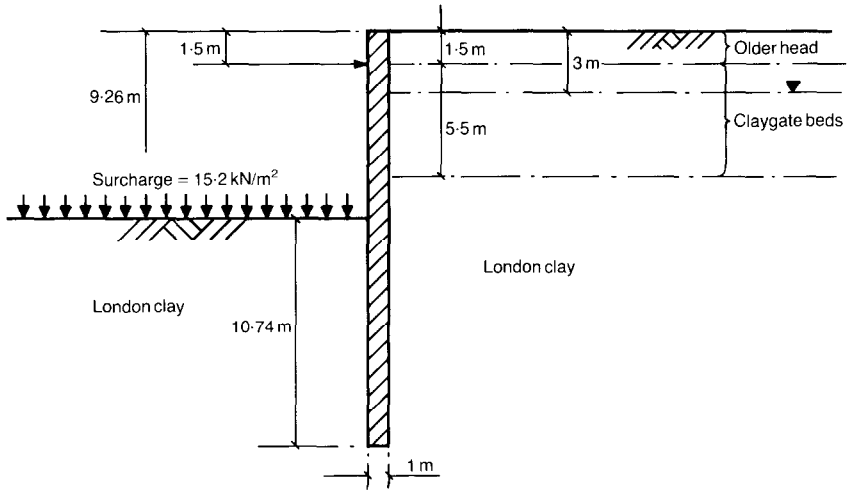

Fig. 23. Idealized geometry of the Bell Common wall, Hubbard *et al.* (1984)

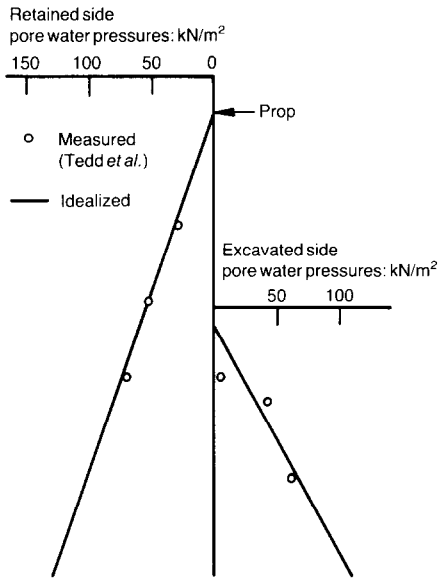

Fig. 24. Measured and idealized pore water pressures at Bell Common, Tedd *et al.* (1984)

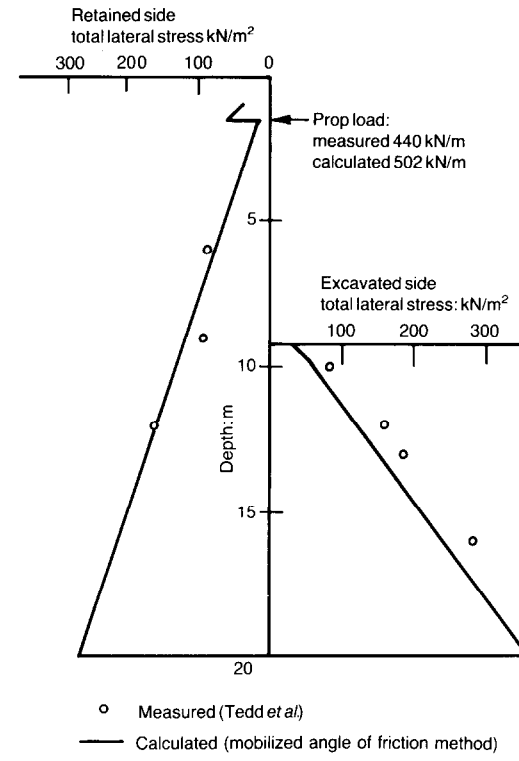

Fig. 25. Measured and calculated total lateral stresses acting on the Bell Common wall, Tedd *et al.* (1984)

The design of the Bell Common tunnel wall was described by Hubbard, Potts, Miller & Burland (1984), and the instrumentation by Tedd, Chard, Charles & Symons (1984) who also reported on the behaviour of the wall between the start of construction (April 1982) and May 1983. The idealized excavation geometry is shown in Fig. 23.

Analysis of the Bell Common wall is complicated by the presence of three distinct soil types on the retained side. Given appropriate laboratory test data, allowance could be made for the different behaviour of the three soils. However, in the following calculations any such difference has been neglected.

The lateral earth pressures were calculated on the assumption that their variation was linear with depth (Fig. 4) using the linear idealizations to the Stage VI pore water pressures measured by Tedd *et al.* (1984) shown in Fig. 24. In the calculation of the effective earth pressure coefficients from the condition of moment equilibrium about the prop, it was assumed that $K_1 = 1/K_2$. Figure 25 shows that the prop load and the total lateral earth pressures thus calculated are close to the values measured by Tedd *et al.*

The pattern of soil movements observed at Bell Common was similar to that observed during the centrifuge test DWC16, the secondary excavations at Bell Common presumably having a similar effect to the slight lack of fit between the props and the wall in test DWC16. It would seem that, given appropriate laboratory test data, the Bell Common wall could be analysed quite fully using the procedures described. The effect of the construction sequence (including secondary excavations such as those made at Bell Common) could also be taken into consideration.

CONCLUSIONS AND SUMMARIZING REMARKS

Kinematically admissible strain fields were derived which idealize soil behaviour in terms of uniformly deforming triangles. Active and passive triangles were defined which are free to slide on vertical and horizontal surfaces but which can be attached to rigid zones through zero extension lines. In the absence of dilation, zero extension lines are at 45° to the principle axes of strain. Any deformation of a rigid retaining wall can be accommodated in this idealized fashion. For example, a field comprising six triangles was used to represent the rotation of an embedded wall about a point above its base. Discontinuities of displacement were seen to have been invoked on the same surfaces as those required in an elementary approach to equilibrium invoking simple active and passive zones.

The strain fields indicated that wall rotation $\delta\theta$ could mobilize a shear strain increment $\delta\gamma = 2\ \delta\theta$ within the neighbouring zones of deformation, whether the wall rotated about the top or the base of the adjacent soil layer. An embedded cantilever was also shown to possess an admissible strain field within which the shear strain also increased everywhere by $2\ \delta\theta$. Only in the case of the passive zone beneath the level of the excavation of a wall propped at its crest did it appear likely that the shear strain increment would be slightly larger.

It has been demonstrated that centrifuge model tests can form the basis of research into soil–structure interaction. It is necessary to simplify the complex of data by imposing upon it certain idealizations which represent the essential behaviour patterns. Such idealizations can lead to the enrichment of engineering design calculations.

However, experimental techniques do need to be refined. Problems of misfit of stiff soil against relatively stiff structures were found to limit the exercise of fine control over kinematic boundary conditions. Methods of grouting and excavation in-flight will have to be developed if more difficult problems are to be researched.

A constant mobilized strength approach was used to back-analyse a group of centrifugal model tests on rigid walls, unpropped or propped. For a particular geometry and groundwater condition, a pair of earth pressure coefficients could be inferred from a simple equilibrium analysis. Curves of ϕ' against γ were insensitive to small changes of overconsolidation ratio and initial effective stress, but plane strain was found to evoke a stiffer response than triaxial strain. Anisotropy was not explicitly dealt with. However, the assumed mobilized shear strain γ was measured and displacements were calculated using an appropriate idealized strain field. When compared with centrifuge test data of soil and wall deformations, the concordance was found to be sufficiently accurate, in the sense that a design based on this approach would have performed at or slightly within the specificied deformation envelope. In this respect the mobilized ϕ approach can be seen to be more useful, reliable and logical than the safety factor approach, without creating any serious difficulties for the designer.

The adoption of geostructural mechanisms in this Paper has followed the spirit of engineers' beam theory. Beam theory neglects shear deformations in favour of a simple mechanistic treatment of bending in terms of plane sections remaining plane. Although 'wrong', engineers' beam theory proves more useful to the designer than more complete approaches, since it characterizes stress and strain in a consistent fashion which is geometrically simple. Experiment proves it to be acceptably accurate for a particular class of beams which are 'slender'.

Designers facing difficulties with soil–structure interaction have suffered from a lack of such simplified treatments. Code formulae have often been based on poorly digested information peculiar to a given site which should not have been applied in other contexts. However, finite element analyses produce such a volume of detailed prediction that patterns are difficult to discern and assumptions (especially of the material stress–strain laws) difficult to evaluate.

Geostructural mechanisms which are based on lower bound stress fields, but which incorporate consistent strain fields, are felt to be a suitable design tool. It has been demonstrated that any desired stress–strain relation could have been used as the basis of prediction, though the technique should lead to the adoption of real data from stress paths appropriate to the problem. Such proposed mechanisms must, of course, be tested. The centrifuge model technique appears suited to this task.

ACKNOWLEDGEMENT

The work reported was carried out under contract to the Transport and Road Research Laboratory (TRRL). The views expressed are not necessarily those of the Department of Transport. W. Powrie received support from the Science and Engineering Research Council.

The Authors are grateful to Mr I. F. Symons (TRRL) for his advice and constructive criticism. We also recognise the support by colleagues in the Soil Mechanics Group at Cambridge, and in particular the assistance of Mr C. H. Collison, Mr J. Doherty and Mr D. I. Stewart.

APPENDIX 1: EQUILIBRIUM CALCULATION FOR A WALL PROPPED AT THE CREST

Figure 26 shows the distributions of pore water pressure and horizontal effective stress assumed to be acting on each side of the wall. Taking moments about the prop yields

$$\left[K_1 \bar{u}_{T_1} \frac{(h+d)^2}{2}\right] + \left[\frac{K_1}{3}(h+d)^2(\gamma_{sat}(h+d) - u_{B_1} - \bar{u}_{T_1})\right] + \left[\frac{(h+d)^2}{3}(u_{B_1} + \bar{u}_{T_1})\right] - \left[\frac{(h+d)^2}{2}\bar{u}_{T_1}\right] = \left[K_2 \bar{u}_{T_2} d\left(h + \frac{d}{2}\right)\right]$$

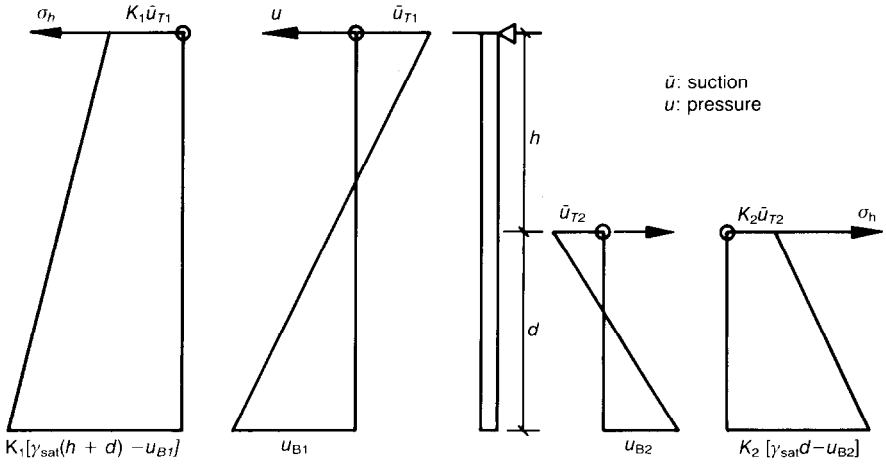

Fig. 26. Pore pressure and effective stress distributions

$$+\left[\frac{K_2}{2}d\left(h+\frac{2d}{3}\right)(\gamma_{sat}d-u_{B_2}-\bar{u}_{T_2})\right]$$

$$+\left[\frac{d}{2}(u_{B_2}+\bar{u}_{T_2})\left(h+\frac{2d}{3}\right)\right]-\left[d\bar{u}_{T_2}\left(h+\frac{d}{2}\right)\right] \quad (22)$$

If $K_1 = K = 1/K_2$, this equation reduces to a quadratic in K (the values of $\bar{u}_{T_1}$, u_{B_1}, $\bar{u}_{T_2}$, u_{B_2}, γ_{sat}, h and d being known). A different relationship between K_1 and K_2 might be assumed (for example, to take account of the effects of wall friction) in which case an iterative method of solution would probably be necessary.

The total lateral stress is negative (tensile) on the retained side of the wall above a depth given by

$$z_0 = \frac{\bar{u}_{T_1}(1-K_1)(h+d)}{[K_1(\gamma_{sat}(h+d)-u_{B_1}-u_{T_1})]+u_{B_1}+\bar{u}_{T_1}} \quad (23)$$

For a surface suction $\bar{u}_{T_1} = 20$ kN/m^2, z_0 is likely to be of the order of 0·8 m, and if $\bar{u}_{T_1} = 100$ kN/m^2, $z_0 =$ 3 m. For the purpose of back-analysis, these figures were not considered to be unreasonable and a 'no-tension' cut-off was not applied.

APPENDIX 2: CALCULATION OF PORE WATER PRESSURES IMMEDIATELY AFTER EXCAVATION

If the soil is assumed to behave as an isotropic and reversibly elastic material, the changes in pore water pressure induced on excavation may also be calculated, on the basis that the average effective stress p' remains the same. Before excavation, it is supposed that the lateral earth pressure coefficient is unity and that the pore water pressure at a depth z below the retained soil surface is given by $u_1 = \gamma_w z - \bar{u}_{r_1}$, where $\bar{u}_{r_1}$ is the pore water suction at the surface. Then, initially at a depth z, $p' = (\gamma_{sat} - \gamma_w)z + \bar{u}_{r_1}$. After excavation, it is supposed that the pore water pressure at a depth z is u_2, the coefficient of lateral earth pressure in the direction perpendicular to the face of the wall is K, and that the effective stress in the longitudinal direction is equal to the mean effective stress $\sigma_v'(K+1)/2$.

Then, at a depth z on the retained side of a frictionless wall, the average effective stress is given by $p' = (K+1)(\gamma_{sat}z - u_2)/2$ so that

$$u_2 = \left[\gamma_{sat} - \frac{2(\gamma_{sat}-\gamma_w)}{K+1}\right]z - \frac{2\bar{u}_{r_1}}{K+1} \quad (24)$$

Similarly, at a depth z below the soil surface on the excavated side of the wall

$$u_2 = \left[\gamma_{sat} - \frac{2(\gamma_{sat}-\gamma_w)}{K+1}\right]z + \left[\frac{2}{K+1}(u_{e_1} - 10\gamma_{sat})\right] \quad (25)$$

where u_{e_1} is the pre-excavation pore water pressure at the level of the excavation, and the depth of the excavation is 10 m. If the wall is perfectly rough, so that $\delta = \phi'_{mob}$ these expressions become

$$u_2 = \left[\gamma_{sat} - \frac{\cos^2\phi'_{mob}}{K}(\gamma_{sat}-\gamma_w)\right]z - \frac{\cos^2\phi'_{mob}}{K}\bar{u}_{r_1} \quad (26)$$

On the retained side of the wall, and

$$u_2 = \left[\gamma_{sat} - \frac{\cos^2\phi'_{mob}}{K}(\gamma_{sat}-\gamma_w)\right]z + \frac{\cos^2\phi'_{mob}}{K}(u_{e_1} - 10\gamma_{sat}) \quad (27)$$

on the excavated side, where $K = \sigma_h'/(\gamma_{sat}z - u_2)$

REFERENCES

Al-Tabbaa, A. (1987). Permeability and stress–strain response of speswhite kaolin. PhD thesis, Cambridge University.

Bolton, M. D. & Powrie, W. (1987). Collapse of diaphragm walls retaining clay. *Géotechnique* **37**, No. 3, 335–353.

Bolton, M. D., Powrie, W. & Stewart, D. I. (1987). Effects on diaphragm walls of groundwater pressure rising in clays. *Proc. 9th Eur. Conf. Soil Mech. Fdn Engng* **2**, 759–762.

Bransby, P. L. & Milligan, G. W. E. (1975). Soil deformations near cantilever sheet-pile walls. *Géotechnique* **25**, No. 2, 75–195.

Burland, J. B. & Hancock, R. J. R. (1977). Underground car park at the House of Commons–geotechnical aspects. *Struct. Engr* **55**, 87–100.

Burland, J. B., Potts, D. M. & Walsh, N. M. (1981). The overall stability of free and propped embedded cantilever retaining walls. *Ground Engng* **14**, No. 5, 28–38.

Burland, J. B., Simpson, B. & St. John, H. D. (1979). Movements around excavations in London clay. *Proc. 7th Eur. Conf. Soil Mech., Brighton* **1**, 13–29.

Caquot, A. & Kerisel, J. (1948). Tables for the calculation of passive pressure, etc. Paris: Gauthier Villars.

Hubbard, H. W., Potts, D. M., Miller, D. & Burland, J. B. (1984). Design of the retaining walls for the M25 cut and cover tunnel at Bell Common. *Géotechnique* **34**, No. 4, 495–512.

James, R. G., Smith, I. A. A. & Bransby, P. L. (1972). Prediction of stresses and deformations in a sand mass adjacent to a retaining wall. *Proc. 5th Eur. Conf. Soil Mech., Madrid* **1**, 39–46.

Milligan, G. W. E. & Bransby, P. L. (1976). Combined active and passive rotational failure of a retaining wall in sand. *Géotechnique* **26**, No. 3, 473–494.

Potts, D. M. & Fourie, A. B. (1984). The behaviour of a propped retaining wall: results of a numerical investigation. *Géotechnique* **34**, No. 3, 383–404.

Powrie, W. (1985). Discussion on Fifth Géotechnique Symposium in Print. The performance of propped and cantilevered rigid walls. *Géotechnique* **35**, No. 4, 546–548.

Powrie, W. (1986). *The behaviour of diaphragm walls in clay*. PhD thesis, Cambridge University.

Rowe, P. W. (1952). Anchored sheet pile walls. *Proc. Inst. Civ. Engrs, Pt 1*, **1**, 27–70.

Rowe, P. W. (1955). Sheet pile walls encastré at the anchorage. *Proc. Inst. Civ. Engrs, Pt 1*, **4**, 70–87

Schofield, A. N. (1980). Cambridge geotechnical centrifuge operations. 20th Rankine Lecture. *Géotechnique* **30**, No. 3, 227–267.

Tedd, P., Chard, B. M., Charles, J. A. & Symons, I. F. (1984). Behaviour of a propped embedded retaining wall in stiff clay at Bell Common tunnel. *Géotechnique* **34**, 513–532.

Ward, W. H. (1961). Displacements and strains in tunnels beneath a large excavation in London. *Proc. 5th Int. Conf. Soil Mech. Fdn Engng, Paris* **2**, 749–753.